Progress of Theoretical Physics, Vol. 13, No. 4, April 1955

Nuclear Reactions at Moderate Energies and Fermi Gas Model

Satio HAYAKAWA,* Mitsuji KAWAI** and Ken KIKUCHI***

* *Research Institute for Fundamental Physics, Kyoto University*
** *Institute of Science and Technology, University of Tokyo*
*** *Department of Physics, Osaka University*

(Received February. 24 1955)

The cross section for nucleon-nucleon collisions in the nuclear matter is calculated in an analytical way on the basis of the Fermi gas model and the inverse energy nucleon scattering cross section. The mean free path thus derived is found to be in qualitative agreement with those deduced from the phenomenological analyses of scattering experiments at low as well as at moderate energies. The angular and energy distributions of knock-out nucleons are calculated and allow us to predict the contribution of such direct collisions to nuclear reactions. For the bombardment of 18 Mev protons on iron this contribution to the energy spectrum of emitted protons is found far smaller than that from the evaporation process. Nevertheless, this influence is not negligible in deducing the nuclear temperature. For the bombardment of 31 Mev protons the knock-out process can account for the gross behaviour of high energy nucleons observed in experiments.

§ 1. Introduction and summary

Recent experiments[1-2] on the inelastic scattering of protons at an intermediate energy range have suggested that the compound nucleus theory might be insufficient to account for their experimental results. In fact, it has been pointed out by several authors[3-5] that the discrepancies berween the theory and the experiments might be due to the neglect of the contribution from the directly knocked-out nucleons in the theoretical calculation. It is, however, difficult to carry out an accurate estimate of this effect since our knowledge about the nuclear structure is at present very scanty. Therefore, we are obliged to adopt a specific model to perform the theoretical analysis for investigating the real features of nuclear reactions. It is well known that no particular nuclear model can sufficiently account for the great variety of nuclear phenomena, but a specific model should be chosen according to the phenomenon concerned. Among various models thus far proposed, experiences tell us that the Fermi gas model is unexpectedly valid in a wide range of phenomena. The merit of this model is further amplified by its simplicity and easy applicability to practical problems. A number of works based on the Fermi gas model have thus been carried out and found to be successful in explaining the qualitative properties of nuclear phenomena. Encouraged by such successes and motivated by the recent experiments, we shall extend the kinematical works on the Fermi gas model, so as to be applicable to a wider range of phenomena.

In § 2 and § 3 are derived the mean free parh of a nucleon in the nuclear matter

and the energy distribution of nucleons knocked out by an impinging nucleon. The analytical treatment of these problems has first been given by Goldberger[6] in order to interpret the nuclear reactions induced by 90 Mev neutrons. In his analytical calculation was assumed for the nucleon-nucleon scattering the energy-independent and isotropic cross section that did not correspond to the experimental evidences. The real form of the cross section has been regarded to be very complicared as to forbid the analytical calculation and has been handled only with the Monte Carlo method.[7] The latter method is accurate so long as a great number of paths are traced, but is not always practicable to get the results covering a wide energy range. Accordingly, we shall here attempt to perform an analytical calculation, dropping the assumption of the energy-independent cross section but still keeping that of the isotropic one, since the latter holds at low energies and even at high energies for the proton-proton scattering.

At low energies where the energy of a nucleon inside a nucleus is below twice the Fermi energy, the analytical calculation of the mean free path of a nucleon was carried out by Yamaguchi[8] on the basis of the above two simplifying assumptions. However, his result is found to be in error. We shall give the correct expressions in (2·8) and (2·10) with (2·11) for such a quantity together with the computational device in this energy region.

The mean free path thus obtained is in approximate agreement with the one obtained by the Monte Carlo calculation (Fig. 1). Our result is compared with the absorption coefficient deduced by Taylor[9] from high energy transmission experiments in one hand, and with the complex potential proposed by Feshbach, Porter and Weisskopf[10] at low energies on the other hand (Fig. 2). The agreement is not very good, but seems to be satisfactory on account of the oversimplification in our model. Further, our result is applied to such a discussion for the validity of the independent particle model as has been pointed out by Weisskopf.[11]

One might, however, wonder the applicability of the Fermi gas model at zero temperature to such low energy phenomena, since the momentum distribution of nucleons is known to be different from that in the Fermi gas at zero temperature on the theoretical as well as experimental grounds. Indeed, this has led Kind and Perganini[12] to considering the mean free path in the Fermi gas at finite temperature. This, however, should not be attributed to the finiteness of temperature, but to the deviation of nucleon waves from plane waves due to the rather strong interactions. It is, therefore, not correct to work with the classical particle picture, as Kind and Perganini did, when the momentum distribution is different from that of the free gas at zero temperature, but one has to do with the distorted wave function of nucleons within the nucleus. Since a great complexity is introduced in the calculation by such a modification, we think it a consistent way to work with the classical particle picture together with the Fermi gas at zero temperature. In fact, our roughness in the model is partially compensated by the internal consistency of our method of treatment and provides a useful basis for the future development of theoretical investigations of the concerned phenomena.

We have also dealt with the energy distribution of nucleons knocked out by nucleons

of moderate energies ((3·14) and Fig. 3–6). The energy distribution under consideration is usually considered to be governed mainly by the evaporation of nuclear particles and partly by the reaction taking place at the nuclear surface, which has been analysed by Austern *et al.*[13] The importance of the knock-out process has first been recognized by Bernardini *et al*[7] through their Monté Carlo calculation. This effect is shown to be diminished due to the surface transmission but not to be negligible yet.[12] Moreover, in the actual nuclear reaction the attenuation of both impinging and scattered beams is not negligible for the reason that the mean free path is much smaller than the nuclear radius in the energy range concerned here. In § 4 we examine in detail these effects in the application of our model to the energy spectra of nucleons from Fe bombarded by 18 Mev protons (Fig. 8–10). Our semi-classical method is essentially the same as in the Monté Carlo works, except that we take into account the refraction of nucleon beam at the nuclear boundary.

The small difference in proton yields between the forward and the backward directions in the 18 Mev proton inelastic scattering predicts that the proton yield due to the evaporation process is actually predominant over that due to the knock-out process. The energy spectra of nucleons observed in the experiment are attributed to many possible types of decay processes, in which, therefore, it is necessary to calculate the cross section of various processes of nucleon emission to make a careful comparison between the theoretical and the experimental results. In view of the above situations, our calculation is performed in § 5, using the compound nucleus formalism, with the semi-empirical formula for the nuclear level densities (Fig. 11–19). The parameters in the nuclear level density formula have usually been determined, disregarding the knock-out process, with the aid of the experimental energy spectrum and the evaporation model. Accordingly, one of the parameters which we have adopted is not always accurate, but we shall proceed our investigation for the two available values of the level density parameter to examine the ambiguity which might be caused by its inaccuracy. The calculated energy spectra are actually found to become different from the Maxwellian type in their shapes, because of the secondary emission of particles from intermediate residual nuclei. The residual nuclei after the first evaporation as well as the knock-out processes are often so highly excited that they can emit particles on returning to the ground state. These cross sections are also estimated in § 5 (Table 1).

Further our results facilitate to discuss the energy dependence of the nuclear temperature on the basis of the energy spectrum obtained. From the theoretical analysis Lang and Le Couteur[14] have called attention to the difference between the true temperature and the apparent one. This discrepancy, however, seems to be insufficient to explain the queer tendency of the nuclear temperature pointed out by Cohen[15] (Fig. 20). On the other hand, Tomasini[16] has shown that the second neutron in $(n\,;\,2n)$ reactions can not be negligible in the determination of the nuclear temperature. A similar situation happens such that the second particles after the direct nucleon emission play a role to describe the behavior of the nuclear temperature. In spite of the small magnitude of the cross section for the knock-out process, the nucleons directly knocked out turn to be a cause of the strange energy dependence of the temperature, which is explainable in this term only in

the forward direction (at $\theta=60°$). Though the difficulty remains concerning the backward direction, this success suspects that some similar processes are likely to give a small yield to the backward scattering.

The remarkable anisotropy in the angular distribution of protons from several elements when bombarded by 31 Mev protons[2] suggests us that the knock-out process might give the main contribution to the nuclear reaction in such a high energy range. Although the proton emission is less probable than the neutron emission according to the compound nucleus formalism, the large magnitude of $(p\,;\,p')$ cross section also seems to assure us that the direct process plays an important role in the actual nuclear reaction. In view of such situations we shall apply our model to the inelastic scattering of 31 Mev protons by Sn in § 6, in which our estimate, though a very crude one, shows a fair agreement with the experimental data (Fig. 22).

§ 2. Mean free path of nucleons in the nuclear matter

According to the Fermi gas model of nucleus, each nucleon is considered to be a classical particle moving in a constant potential. The momentum and the kinetic energy (non-relativistic) of a nucleon is measured in nuclei, *i.e.*, from the bottom of the potential, if not specially mentioned, taking the nucleon mass to be unity. Let the momenta of incident and target nucleons be $\boldsymbol{P}_1$ and $\boldsymbol{P}_2$ and those of an outgoing and residual nucleon be $\boldsymbol{P}_1'$ and $\boldsymbol{P}_2'$, respectively. The Fermi gas at zero temperature gives rise to a uniform distribution of $\boldsymbol{P}_2$ restricted by the Fermi momentum $\boldsymbol{P}_F$. The Pauli principle requires $|\boldsymbol{P}_1'|>P_F$ and $|\boldsymbol{P}_2'|>P_F$.

The scattering cross section for these nucleons is a function of half the relative momenta of the initial and final states, $\boldsymbol{P}$ and $\boldsymbol{P}'$, respectively. Since these are the same in the laboratory system as in the center of mass one, the difference in the differential cross section $\sigma(\boldsymbol{P},\boldsymbol{P}')d\Omega'$ in the two coordinate systems is entirely due to the difference in the solid angle elements, $d\Omega'$, for $\boldsymbol{P}'$. On account of the collision frequency obtained with the multiplication by the relative velocity $2P=2|\boldsymbol{P}|$, the total nucleon-nucleon cross section in nuclear matter is given by

$$\bar{\sigma}=\frac{1}{P_1(4\pi/3)P_F^3}\int d\boldsymbol{P}_2\int d\Omega' 2P\sigma(\boldsymbol{P},\boldsymbol{P}'). \qquad (2\cdot1)$$

$\sigma(\boldsymbol{P},\boldsymbol{P}')$ in the center of mass system depends on $|\boldsymbol{P}|$ approximately as P^{-2} over a considerably wide range of energies and also on the angle between $\boldsymbol{P}$ and $\boldsymbol{P}'$ for neutron-proton scattering. The latter dependence may, however, be neglected with a small error, because the Pauli principle will make the small angle scattering relatively unimportant. Thus we may be allowed to assume

$$\sigma(\boldsymbol{P},\boldsymbol{P}')=\sigma_t(P)/4\pi\,, \qquad (2\cdot2)$$

where $\sigma_t(P)$ is the total cross section for a nucleon of relative momentum $\boldsymbol{P}$.

From now on we can work out in the laboratory system, taking the invariant cross section $\sigma_t(P)$ outside of the integral over Ω' which is now reduced simply to a factor,

i.e., the solid angle Ω' covered by possible final directions of $\boldsymbol{P}'$. Taking into account the Pauli principle for $\boldsymbol{P}_1'$ and $\boldsymbol{P}_2'$, we have

$$\Omega' = 4\pi \frac{P_1^2 + P_2^2 - 2P_F^2}{2P|\boldsymbol{P}_1 + \boldsymbol{P}_2|} . \tag{2·3}$$

$\Omega' \leq 0$ restricts the integration region over $\boldsymbol{P}_2$ as

$$P_2^2 \geq 2P_F^2 - P_1^2 . \tag{2·4}$$

(2·4) gives us the ranges of integration, according to the magnitude of P_1^2, as

$$\begin{aligned} &0 \leq P_2^2 \leq P_F^2 \qquad \text{for} \quad P_1^2 \geq 2P_F^2, \qquad \text{(I)} \\ &2P_F^2 - P_1^2 \leq P_2^2 \leq P_F^2 \qquad \text{for} \quad P_1^2 \leq 2P_F^2. \qquad \text{(II)} \end{aligned} \tag{2·5}$$

With the use of (2·3) and these integral limits, (2·1) is reduced to

$$\bar{\sigma} = \frac{1}{P_1 (4\pi/3) P_F^3} \int \frac{P_1^2 + P_2^2 - 2P_F^2}{|\boldsymbol{P}_1 + \boldsymbol{P}_2|} \sigma_t(P) d\boldsymbol{P}_2 . \tag{2·6}$$

In accordance with Goldberger,[6] we shall, for the time being, assume the energy independence of the cross section $\sigma_t(P)$, in which case the angular integration in (2·6) is readily carried out as

$$\int_0^{\pi} \frac{\sin\theta \, d\theta}{|\boldsymbol{P}_1 + \boldsymbol{P}_2|} = \int_{-1}^{1} \frac{dx}{\sqrt{P_1^2 + P_2^2 - 2P_1 P_2 x}} = \frac{2}{P_1} . \tag{2·7}$$

Introducing this into (2·6) and taking into account (2·5), we obtain

$$\bar{\sigma} = \begin{cases} \sigma_t \left(1 - \dfrac{7}{5} \cdot \dfrac{E_F}{E_1}\right) & \text{for} \quad E_1 \geq 2E_F , \qquad \text{(I)} \\ \sigma_t \left\{1 - \dfrac{7}{5} \cdot \dfrac{E_F}{E_1} + \dfrac{2}{5} \cdot \dfrac{E_F}{E_1} \left(2 - \dfrac{E_1}{E_F}\right)^{5/2}\right\} & \text{for} \quad E_1 \leq 2E_F . \qquad \text{(II)} \end{cases} \tag{2·8}$$

Here the cross section is expressed in terms of energies,

$$E_1 = P_1^2/2 , \quad E_F = P_F^2/2 .$$

(2·8, I) is nothing but the one obtained by Goldberger,[6] but our way of derivation is much simpler. The cross section for energy range (II) was given by Yamaguchi,[8] whose result, however, is not in agreement with (2·8, II).

Now we shall drop the assumption on the energy independence of $\sigma_t(P)$ in the evaluation of (2·6). The total cross section is known to be inversely proportional to the incident energy ($\propto P^{-2}$) over a considerable range of energies. Hence we assume

$$\sigma_t(P) = \sigma_0 / P^2 . \tag{2·9}$$

Substituting this into (2·6), we get

$$\sigma = 6\sigma_0 P_1 \boldsymbol{I} / P_F^3 . \tag{2·10}$$

$\boldsymbol{I}$ is given by a complicated integral

$$\boldsymbol{I} = \int_a^b \frac{x(1 + x^2 - 2\alpha^2)}{\sqrt{2(1+x^2)}} \tanh^{-1} \frac{2x\sqrt{2(1+x^2)}}{1+3x^2} \, dx , \tag{2·11}$$

where

$$x=P_2/P_1\,,\quad \alpha=P_F/P_1$$

and the integration limits are

$$\begin{aligned} &a=0\,,\quad b=\alpha && \text{for}\quad E_1\geq 2E_F\,, && \text{(I)}\\ &a=\sqrt{2\alpha-1}\,,\quad b=\alpha && \text{for}\quad E_1\leq 2E_F\,, && \text{(II)} \end{aligned} \qquad (2\cdot12)$$

respectively.

In an actual nucleus which consists of N neutrons and Z protons, the average cross section should be given by

$$\bar{\sigma}=(N\bar{\sigma}_{ni}+Z\bar{\sigma}_{pi})/A\,, \qquad (2\cdot13)$$

where i stands for p or n, according as the incident nucleon is proton or neutron. $\bar{\sigma}_{ni}$ and $\bar{\sigma}_{pi}$ are obtained from (2·1) by putting $\sigma(\boldsymbol{P},\boldsymbol{P}')$ equal to the cross sections for free $n-i$ and $p-i$ collisions respectively. For the numerical works we have taken $N=Z=A/2$ and $E_F=21.5$ Mev and expressed the results in terms of the mean free path λ.

$$\lambda=1/\rho\bar{\sigma}\,, \qquad (2\cdot14)$$

where ρ is the density of nuclear matter.

The calculated mean free paths are shown, in Fig. 1, for both cases of the energy independent and the inverse energy proportional cross sections. For the former case σ_i is taken as the value at the incident energy. These are qualitatively similar to one another in energy dependences but different in magnitudes approximately by 20%, which is ascribed to the fact that the scattering is more suppressed due to the Pauli principle at lower energies where the cross section for free nucleons is larger. In comparing these with the Monté Carlo result by Morrison *et al.*,[17] the case of the inverse energy law is nearer to the Monté Carlo one than the energy independent one, although there is still a small difference in the former case. The reason is that the larger cross section at small angles is relatively ineffective, so that our total cross section is larger than the average over the angular distribution in the nuclear matter. We shall, therefore, have to take the effective total cross section

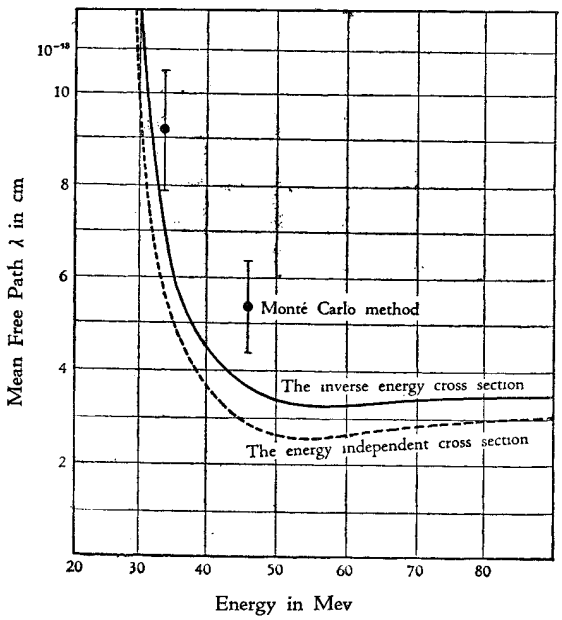

Fig. 1. Mean free path λ *vs.* nucleon energy in the nucleus. Solid curve and dashed curve refer to results calculated on the assumption of the inverse energy and the energy independent cross sections respectively. ⊥: calculated by the Monté Carlo method.

as smaller by about 20% than the observed total cross section.

Above $E_1=50$ Mev, the mean free path turns to increase, as the free cross section decreases and, above 80 Mev, our result can be compared with the absorption mean free path analyzed by Taylor.[9] (Fig. 2)

At low energies, near $E_1=30$ Mev, the phenomenological theory based upon the complex nuclear potential model proposed by Freshbach *et al.*[10] gives the absorption mean free path of 2.4×10^{-12} cm, whereas our calculation with the inverse energy law predicts $0.5\sim1\times10^{-12}$ cm at about this energy. On account of the over-simplification in our calculation, the comparison of these two figures suggests us that the behaviour of the nuclear potential can be understood in terms of the Fermi gas model even at such low energies. This might be rather surprising in view of the strong interaction of nucleons with nuclear matter, but the Pauli principle is taken to play an essential role in weakening the effective nuclear interactions. This fact may be supposed to lead to the validity of the optical model at low energies.

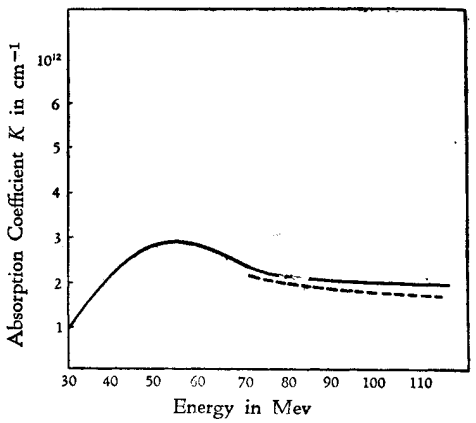

Fig. 2. Absorption coefficient $K(=\lambda^{-1})$ *vs.* nucleon energy in the nucleus. Solid curve indicates the calculated result with the inverse energy cross section and dashed one is that obtained by Talor[9] through the analysis of the neutron-nucleus scattering.

The mentioned success in accounting for the optical model allows us to infer the possibility of describing some of lower energy levels in terms of the Fermi gas model. For this purpose we derive the collision width for a single nucleon from (2·8, II) as

$$\Gamma_c=\bar{\sigma}\rho v_1\hbar\simeq(3/4)\sigma_t\rho v_1\hbar(E_1-E_F)^2/E_F^2 \qquad (2\cdot15)$$

assuming the energy independent cross section and $E_1-E_F\ll E_F$. Here $\rho=1.4\times10^{38}$ cm^{-3} is the nucleon density in nuclei and $v_1\simeq c/4$ the velocity of the incident nucleon. Taking $\sigma_t\simeq0.2$ barn and $(E_1-E_F)/E_F\simeq1/5$, Γ_c is estimated as about 4 Mev. This may be compared with the level distance D which represents the reciprocal period of such motion that constitutes the levels concerned. If the single particle motion in a nucleus persists long enough to constitute an energy level, Γ_c should be smaller than D. This barely holds merely for the lowest levels of leight nuclei. Neverthless, the single particle model may still be justified, if one notices that D should be the level distance of single particle levels only. Then D is larger than the average level distance of all observed levels and may satisfy $D>\Gamma_c$, provided that excitation energies are low enough. Our over-simplified theory prevents us to go farther, but the strong energy dependence shown in (2·15) will make one understand the increasing validity of the single particle description with decreasing excitation energies.

§ 3. Energy distribution of the scattered particle due to the single collision

In this section we shall investigate the energy spectrum and angular distribution of scattered nucleons, after a single collision in the nucleus, on the basis of the same model and the similar assumption of (2·2) as in the preceding section. The result will allow us to examine the effect, on this process, of the energy dependence of the free nucleon-nucleon collision cross section, comparing our result with that of Goldberger's.

We shall employ the notation $\boldsymbol{P}_f$ to indicate the final momentum of the particle under consideration in order to facilitate the calculations in the collisions between like particles in which case we have no means to discriminate which of the collision partners we are observing. Accordingly, we denote by $\boldsymbol{P}_2'$ the final momentum of the rest of the collision partners.

The differential cross section $\sigma(\boldsymbol{P}_f)d\boldsymbol{P}_f$ for the scattered particle having the final momentum between $\boldsymbol{P}_f$ and $\boldsymbol{P}_f+d\boldsymbol{P}_f$ in the laboratory system is given by the formula

$$\sigma(\boldsymbol{P}_f)d\boldsymbol{P}_f=\frac{1}{v_1(4\pi/3)P_F^{\,3}}\int v_{\rm rel}\,\sigma(\boldsymbol{P},\boldsymbol{P}')\frac{\delta(P-P')}{P^2}d\boldsymbol{P}_2 d\boldsymbol{P}_f\,. \tag{3·1}$$

On account of the relations

$$\delta(P'-P)=2P\delta(P'^2-P^2),$$

$$v_{\rm rel}=2P,$$

(3·1) can be rewritten as

$$\sigma(\boldsymbol{P}_f)d\boldsymbol{P}_f=\frac{4}{v_1(4\pi/3)P_F^{\,3}}d\boldsymbol{P}_f\int\sigma(\boldsymbol{P},\boldsymbol{P}')\,\delta(P^2-P^2)\,d\boldsymbol{P}_2\,. \tag{3·2}$$

In contrast to the calculation of the effective total cross section in the preceding section, it is, in the present case, convenient to proceed just as Goldberger has done. Thus we introduce the cylindrical coordinate system whose polar axis lies along the direction of the momentum transfer vector,

$$\boldsymbol{q}=\boldsymbol{P}_f-\boldsymbol{P}_1 \tag{3·3}$$

and whose origin is situated at the centre of the Fermi sphere. In terms of the coordinate (z,ρ,φ) instead of (P_{2x},P_{2y},P_{2z}), we can rewrite the argument P'^2-P^2 of the δ-function as

$$\delta(P'^2-P^2)=q^{-1}\delta(z-z_0), \tag{3·4}$$

where

$$z_0=\frac{1}{2q}(P_f^2+q^2-P_1^2). \tag{3·5}$$

Assuming, $\sigma(\boldsymbol{P},\boldsymbol{P}')=\sigma_t(P)/4\pi$ as in § 2, we obtain

$$\sigma(\boldsymbol{P}_f)d\boldsymbol{P}_f=\frac{4}{v_1(4\pi/3)P_F^{\,3}}\cdot\frac{1}{2q}\cdot\frac{1}{4\pi}\int\sigma_t(P)\,\delta(z-z_0)\rho\,d\rho\,dz\,d\varphi\,d\boldsymbol{P}_f\,. \tag{3·6}$$

When we further assume that the energy dependence of $\sigma_t(P)$ is unimportant and

put it equal to a constant, then the integration over ρ, z, φ of (3·6) yields the formula obtained by Goldberger.*

Here, however, we shall drop the assumption of the constant cross section mentioned above, putting,

$$\sigma_t(P)=\frac{\sigma_0}{E_{\rm rel}}=\frac{2\sigma_L}{P_1^2+P_2^2-2P_1P_2\cos\alpha}, \tag{3·7}$$

where α is the angle between $\boldsymbol{P}_1$ and $\boldsymbol{P}_2$. σ_L is the total cross section corresponding to the incident energy. Taking $\varphi=0$ in the plane specified by the vectors $\boldsymbol{P}_1$ and $\boldsymbol{q}$, we get

$$\cos\alpha=\sin\zeta\cos\varphi, \tag{3·8}$$

where ζ is the angle between $\boldsymbol{P}_1$ and $\boldsymbol{q}$. Inserting (3·7) and (3·8) into (3·6) and carrying out the integration with respect to φ and z, we have

$$\sigma(\boldsymbol{P}_f)d\boldsymbol{P}_f=\frac{2\sigma_L}{v_1(4\pi/3)P_F^3q}\int\frac{\rho d\rho}{\sqrt{\rho^4+2b\rho^2+c}}d\boldsymbol{P}_f, \tag{3·9}$$

where

$$\begin{aligned} b&=P_1^2+z_0^2-2P_1^2\sin^2\zeta,\\ c&=(P_1^2+z_0^2)^2-4P_1^2z_0^2\sin^2\zeta. \end{aligned} \tag{3·10}$$

The restrictions on P_1 and P_2 are determined by the following condition.

$$P_2^2\leq P_F^2, \quad P_2^2\geq P_F^2; \tag{3·11}$$

the former being the condition that the target nucleon 2 is below the Fermi surface before the collision and the latter expressing the Pauli principle. (3·11) leads to

$$P_F^2+P_f^2-P_1^2-z_0^2\leq\rho^2\leq P_F^2-z_0^2. \tag{3·12}$$

Thus, the limits of integration over ρ are given by

$$\rho_2^2=P_F^2-z_0^2, \tag{3·13a}$$

$$\rho_1^2=\begin{cases} P_F^2+P_f^2-P_1^2-z_0^2, & \text{(3·13b)}\\ 0, \quad (P_F^2+P_f^2-P_1^2-z_0^2\leq 0). & \text{(3·13c)}\end{cases}$$

Carrying out the integration with respect to ρ, we finally obtain the formula for $\sigma(\boldsymbol{P}_f)d\boldsymbol{P}_f$

$$\sigma(\boldsymbol{P}_f)d\boldsymbol{P}_f=\frac{\sigma_t(E)P_1}{(4\pi/3)P_F^3q}\log\frac{\sqrt{\rho_2^4+2b\rho_2^2+c}+\rho_2^2+b}{\sqrt{\rho_1^4+2b\rho_1^2+c}+\rho_1^2+b}. \tag{3·14}$$

Final momentum $\boldsymbol{P}_f$ is restricted by the condition $\rho_2^2\geq 0$, otherwise $\sigma(\boldsymbol{P}_f)d\boldsymbol{P}_f$ being zero.

The conditions: $P_F^2-z_0^2\geq 0$ and $P_F^2+P_f^2-P_1^2-z_0^2\geq 0$ can also be written down in terms of the momentum transfer as follows. $P_F^2-z_0^2\leq 0$ holds in the case

$$P_F+\sqrt{P_1^2-P_f^2+P_F^2}\geq q\geq\sqrt{P_1^2-P_f^2+P_F^2}-P_F, \tag{3·15}$$

and $P_F^2+P_f^2-P_1^2-z_0^2\geq 0$ holds if and only if

---

* His results contain a small mistake in the expression of $\sigma(\boldsymbol{P}_f)d\boldsymbol{P}_f$ in the cases (2) and (3) of his paper, *i.e.*, the correct expression is as follows.

$$\bar{\sigma}(\boldsymbol{P}_0,\boldsymbol{P})=\frac{3}{P_0}\cdot\frac{\{P^2+P_0^2-2PP_0\cos\theta+(P_0^2P^2\sin^2\theta)/(1-P^2)\}/(1-P^2)}{(P^2+P_0^2-2PP_0\cos\theta)^{3/2}}\sigma$$

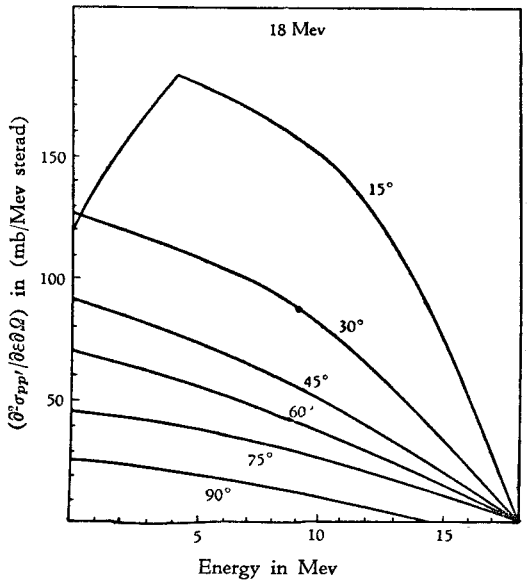

Fig. 3. Energy distribution of protons due to the single collision in the case of the energy independent cross section. The energy of the incident proton is 18 Mev and the target is ^{56}Fe nucleus. Figures attached to respective curves indicate scattered angles.

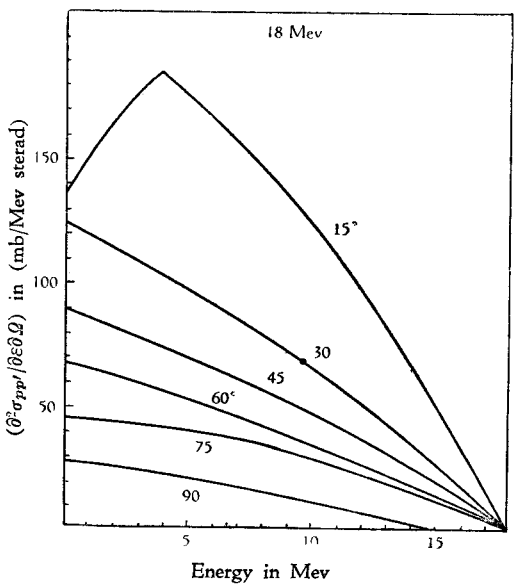

Fig. 4. Energy distribution of protons due to the single collision in the case of the inverse energy cross section. The energy of the incident proton is 18 Mev and the target is ^{56}Fe nucleus. Figures attached to respective curves indicate scattered angles.

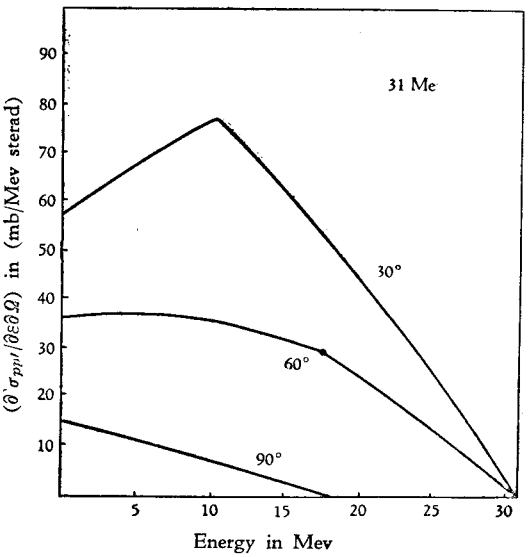

Fig. 5. Energy distribution of protons due to the single collision in the case of the energy independent cross section. The energy of the incident proton is 31 Mev and the target is ^{56}Fe nucleus. Figures attached to respective curves indicate scattered angles.

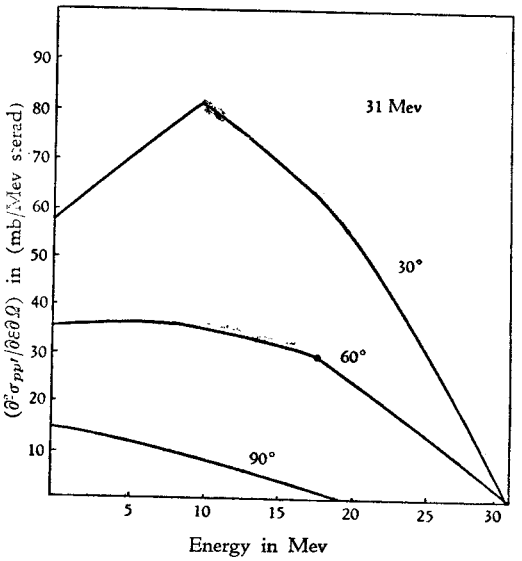

Fig. 6. Energy distribution of protons due to the single collision in the case of the inverse energy cross section. The energy of the incident proton is 31 Mev and the target is ^{56}Fe nucleus. Figures attached to respective curves indicate scattered angles.

$$P_F^2+P_f^2-P_1^2\geq 0$$

and

$$P_F+\sqrt{P_f^2-P_1^2+P_F^2}\geq q\geq P_F-\sqrt{P_f^2-P_1^2+P_F^2}\,. \tag{3·16}$$

The numerical calculations have been performed for the cases of 18 Mev and 31 Mev protons. These results are shown in Fig. 3–6, both for the energy independent and inverse energy cross sections, (2·2).

It should be noticed that the results calculated with the above method fails to give the energy spectrum observed in the experiments for the reason that the effects of transmission and attenuation are not taken into account in the above calculation. These effects shall be treated actually in the next section.

Next we shall examine the mean energy transfer of an incident particle, as is necessary for investigating the effect of the multiple collision on the actual nuclear reactions. Denoting the mean value of the final energy E_f of scattered particles by $\langle E_f\rangle$, the mean energy transfer $\langle E_t\rangle$ is given by

$$\langle E_t\rangle=E_1-\langle E_f\rangle. \tag{3·17}$$

$\langle E_f\rangle$ can be obtained by averaging E_f over the possible directions of the final relative momentum $\boldsymbol{P}'$ and then over the initial momentum $\boldsymbol{P}_2$ of the target nucleon:

$$\langle E_f\rangle=\frac{1}{2}\langle P_f^2\rangle=\frac{1}{2}\cdot\frac{1}{\bar{\sigma}_t(4\pi/3)P_F^3}\iint P_f^2\frac{\sigma_t(P)}{4\pi}2Pd\Omega' d\boldsymbol{P}_f\,, \tag{3·18}$$

where $\bar{\sigma}_t$ is the effective total cross section calculated in § 2, which normalizes the probability density. The calculation is quite analogous to that of the effective total cross section and leads to the following results.

(1) Energy independent cross section:

$$\langle E_f\rangle=\frac{\sigma}{\bar{\sigma}_t}\cdot\frac{1}{\alpha^3}\cdot\frac{1}{2}\int_a^b(1+x^2-2\alpha^2)(1+x^2)x^2dx\cdot E_1\,,$$

where σ_t is the total cross section of free nucleon-nucleon scattering and a, b and α are in (2·12)

In the case of $E_1\geq 2E_F$ (I), the above equation gives

$$\langle E_f\rangle=\frac{E_1}{2}\cdot\frac{1-\frac{4}{5}\cdot\frac{E_F}{E_1}-\frac{27}{35}\left(\frac{E_F}{E_1}\right)^2}{1-\frac{7}{5}\cdot\frac{E_F}{E_1}}, \tag{3·19}$$

while, for $E_1\leq 2E_F$ (II), it leads to

$$\langle E_t\rangle=\frac{E_1}{2}\times\frac{1-\frac{8}{35}(2\alpha^2-1)^{3/2}+\left\{\frac{4}{35}(2\alpha^2-1)^{3/2}-\frac{5}{4}\right\}\frac{E_F}{E_1}+\left\{\frac{4}{35}(2\alpha^2-1)^{3/2}-\frac{37}{35}\right\}\left(\frac{E}{E_1}\right)^2}{1-\frac{7}{5}\cdot\frac{E_F}{E_1}+\frac{2}{5}(2\alpha^2-1)^{5/2}\left(\frac{E_F}{E_1}\right)} \tag{3·20}$$

(2) Inverse energy law:

$$\langle E_f \rangle = \frac{1}{8} \cdot \frac{\boldsymbol{J}}{\boldsymbol{I}} E_1 , \tag{3·21}$$

where $\boldsymbol{I}$ is the integral which already appeared in (2·11) and $\boldsymbol{J}$ is defined by

$$\boldsymbol{J} = \int_a^b (1+x^2-2\alpha^2) \sqrt{2(1+x^2)} \tanh \frac{2x\sqrt{2(1+x^2)}}{1+3x^2} dx \tag{3·22}$$

§ 4. Application of the model to the inelastic scattering of 18 Mev protons by ^{56}Fe —The knock-out process—

In this section we shall make a crude estimate of the contribution due to the knock-out process in the inelastic scattering of protons by Fe. For simplicity, we shall proceed our discussion along the line of a semi-classical approximation, allowing us for the consistency of the model adopted throughout the calculation. In principle, our calculation developed here is the same as Monté Carlo calculation except for taking into account the effects of diffraction and reflection of nucleons over the nuclear surface. In fact, it is easy to see that these effects play important roles particularly in the scattering in the backward direction.

In order to illustrate the main features of the calculations, let us take an example of incident neutrons. Following the semi-classical picture, a neutron or a proton is assumed to have a definite trajectory. Outside the nucleus a neutron travels along a straight line and the flux density through a plane perpendicular to the beam is constant over the whole plane. A beam of neutrons, which strike the nuclear surface at an incident angle, α_i, suffers reflexion and refraction on entering the nuclear medium, because of the difference in the potentials between the outside and the inside of the nucleus. The transmission coefficient $T_i^{(n)}(\alpha_i)$ of the incident neutrons at the nuclear boundary will be calculated in the appendix. It is conveniently expressed in terms of the index of refraction of the nuclear medium.

$$n = k_{\mathrm{in}i}/k_{\mathrm{out}i} \tag{4·1}$$

and the incident angle α_i, where $k_{\mathrm{in}i}$ and $k_{\mathrm{out}i}$ are the wave numbers of the incident neutron inside and outside the nucleus respectively, the suffix i referring to the initial state. The angle of refraction is determined by the well-known Snellius' law

$$k_{\mathrm{out}} \sin\alpha = k_{\mathrm{in}} \sin\beta$$

or

$$\sin\beta = n \sin\alpha . \tag{4·2}$$

The transmitted particle, after running over a distance L_i, the order of mean free path λ_i in the nuclear medium, collides with a nucleon in the nucleus. The mean free paph λ_i, appropriate to the incident energy and the cross section for this elementary collision have been calculated in the previous section. After the collision it will propagate with the wave number $k_{\mathrm{in}f}$ until it reaches the nuclear boundary again. In the course of the

propagation the beam intensity is diminished by a factor $\exp(-L_f/\lambda_f)$, where λ_f is the mean free path appropriate to the final energy $(\hbar^2 k_{\mathrm{in}f}^2/2)$ and L_f is the distance over which the particle has to run before it reaches the nuclear surface. At the boundary it again suffers reflexion and refraction for the same reason as in the case of its entrance into the nuclear matter. These effects are of great importance in the actual reaction. In the extreme case, for instance, in which it reaches the nuclear surface with the incident angel γ_f larger than the critical angle γ_{f0}, defined by the equation

$$\sin\gamma_{f0}=k_{\mathrm{out}f}/k_{\mathrm{in}f}\,, \qquad (4\cdot3)$$

using $k_{\mathrm{out}f}$, *i.e.*, the final momentum of the nucleon outside the nucleus, it can never escape from the nucleus, even if it is energetically possible on account of the perfect reflexion at the surface. Thus the beam intensity is further diminished by a factor $T_f^{(n)}(\delta_f)$, *i.e.*, the transmission coefficient at the nuclear boundary, defined in the same way as $T_i^{(n)}(\alpha_i)$. The situation mentioned above is actually shown in Fig. 7. Summarizing the above considerations, we see that the cross section for this process to occur is given by

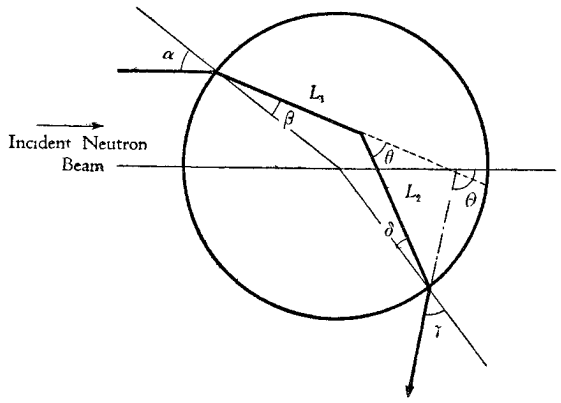

Fig. 7. Schematic representation for the direct process. Both of incident and scattered particles suffer the diffraction and the reflection at the nuclear surface. L_1 and L_2 should be read as L_i and L_f in correspondence to the text.

$$\frac{\partial^2\sigma_d(n\,;\,n)}{\partial\Omega\partial\mathcal{E}}=\frac{\partial}{\partial\Omega}\int d\omega\int d\alpha_i P_i(\alpha_i)\,T_i^{(n)}(\alpha_i)\,\frac{L_i}{\lambda_i}\exp\left(-\frac{L}{\lambda_i}\right)$$
$$\times\frac{\partial^2\sigma_t}{\partial\omega\partial\mathcal{E}_{\mathrm{in}}}\exp\left(-\frac{L_f}{\lambda_f}\right)\cdot T_f^{(n)}(\delta_f)\,, \qquad (4\cdot4)$$

where Ω denotes the solid angle into which the particle is scattered in the final state and $\mathcal{E}$ is its energy outside the nucleus. ω is the solid angle into which the incident nucleon is scattered through a single collision and $\mathcal{E}_{\mathrm{in}}$ its energy inside the nucleus. $P_i(\alpha_i)$ is the probability that an incident particle collides with an angle α_i on the nuclear surface. The differential cross section $(\partial^2\sigma_t/\partial\omega\partial\mathcal{E}_{\mathrm{in}})$ and the mean free paths λ_i and λ_f have been calculated in the preceding sections.

The case of proton incidence can be treated in the same way except for the fact that the path of a proton is distorted from the straight line and the corresponding wave number is not a constant in the outside region of the nucleus, because of the Coulomb potential. Accordingly, Snellius' law is modified as

$$k_{\mathrm{out}}(a)\sin\eta=k_{\mathrm{in}}\sin\beta \qquad (4\cdot5)$$

where $k_{\mathrm{out}}(a)$ is the wave number of the proton at the nuclear boundary and η the incident angle. We shall show, in the appendix, that in our crude approximation, that $k_{\mathrm{out}}(a)$ in (4·5) can be replaced by the wave number $k_{\mathrm{out}\infty}$ of a proton at an infinite distance away

from the nucleus and η by η_∞ which measures the angle between $k_{\text{out}\infty}$ and the normal of the nuclear surface at the incident point of the proton. Namely, we have approximately,

$$k_{\text{out}\infty} \sin\eta_\infty = k_{\text{out}}(a) \sin\eta \qquad (4\cdot6)$$

which leads to the modified Snellius' law of

$$k_{\text{out}\infty} \sin\eta_\infty = k_{\text{in}} \sin\beta\,. \qquad (4\cdot7)$$

From this equation it can be seen that the path of a proton in the nucleus is the same as that of a neutron with the wave number $k_{\text{out}\infty}$ and the incident angle η_∞. Since η_∞ and $k_{\text{out}\infty}$ are known, the calculation can be proceeded in the same way as in the case of the neutron incidence. The transmission coefficient for protons is given in the appendix.

The method mentioned above is applied to work out the inelastic scattering of 18 Mev protons by ^{56}Fe. In our calculation it is assumed, for the sake of simplicity, that collisions always take place when the incident proton has run over a mean free path after entering into the nucleus. Beside this assumption, we have traced a number of proton paths, as they are restricted to a two dimensional plane for computational convenience, just as in the Monté Carlo method. Integrating these together with the weighting factor of (4·4) on each, we obtain finally the effective cross section and the energy spectrum of protons due to the direct process. In this connection, a special attention should be paid to the fact that if the target nucleon is a proton and gets an energy high enough to escape the nucleus after the collision, such a proton is also observed in experiments. In order to take this into account, the proton-proton scattering cross section appearing in the σ_t is multiplied by a factor of 2, as in the usual case of the proton-proton cross section. The calculated result is shown in Fig. 8–9. The energy spectra obtained by integrating over solid angle are shown in Fig. 10.

The total cross sections of the direct processes $\sigma_d(p\,;\,p)$ and $\sigma_d(p\,;\,n)$ are estimated

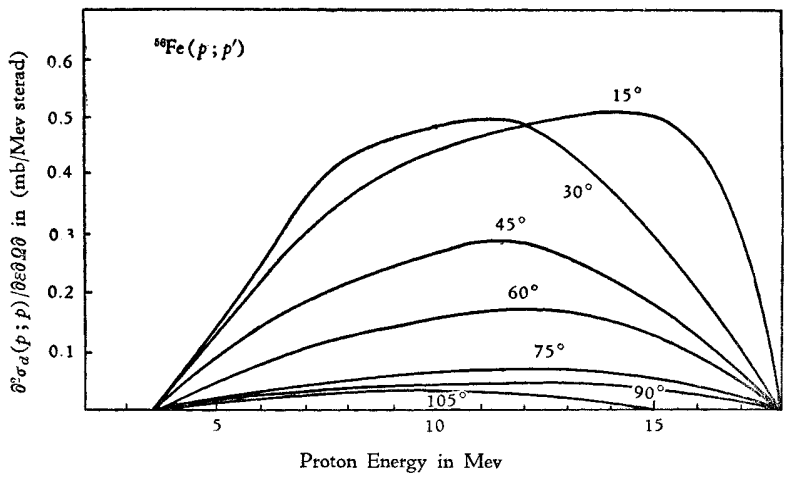

Fig. 8. Energy spectra of protons due to the direct process when 18 Mev protons bombard ^{56}Fe nuclei. Figures attached to respective curves indicate scattered angles.

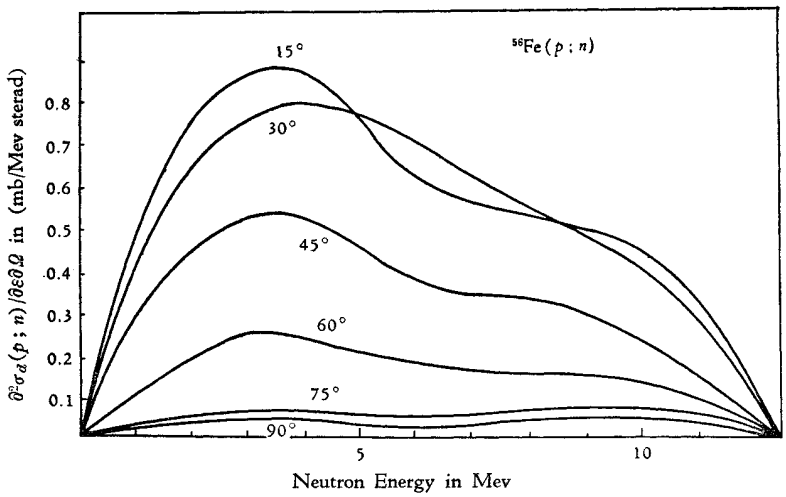

Fig. 9. Energy spectra of neutrons scattered from ^{56}Fe when bombarded by 18 Mev incident protons. Figures attached to respective curves indicate scattered angles.

as 12 mb and 17 mb respectively, which are found to become much smaller than the cross section of the evaporation process as calculated later.

The effect of multiple reflexion at the nuclear boundary before a collision is of little importance, because the mean free path of incident protons in the energy range concerned is of the order of 3×10^{-13} cm, which is smaller than the nuclear radius.

The effect of multiple collision in the nucleus can also be neglected, for the mean energy transfer per collision is approximately 17 Mev according to (3·19), so that after two successive collisions the nucleon loses too large an energy to escape the nucleus.

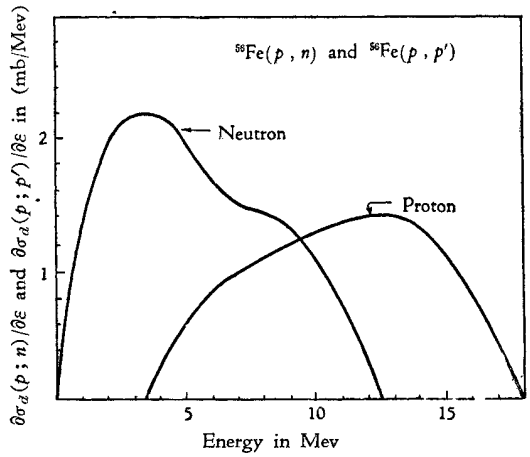

Fig. 10. Energy spectra (integrated over angle) of nucleons scattered from ^{56}Fe when bombarded by 18 Mev protons. Curves give also the distribution of excitation energies in residual nuclei after the direct process.

In connection with the problem of nuclear temperature the proton yield at 150° has been examined, since the available experimental data are concerned with backward scattering, and the differential cross section has been shown to become of the order of 10^{-3} mb/(sterad Mev) for 6 Mev outgoing protons. Protons with higher energies can not be scattered into such a backward direction because of the energy-momentum conservation. The small yield fails to affect appreciably the energy spectrum, so that the behavior of the nuclear temperature may not be altered.

§ 5. The spectra of nucleons emitted through the evaporation and discussions on the nuclear temperature

The purpose in this section is to calculate the energy spectra of nucleons from Fe bombarded by 18 Mev protons on the basis of the evaporation theory. Our method of treatment is essentially the same as that in the previous works,[18,19] which are cited as I and II in the following. We shall, therefore, present only briefly the procedure of our calculations.

According to the compound nucleus formalism, the cross sections for various competing processes are given in terms of the nuclear level density. We shall here employ the following semi-empirical formula of the level density of a nucleus, which is based on the Fermi gas model.

$$w(E) = c \exp 2\sqrt{aE} \tag{5·1}$$

with

$$c_{\text{even-even}} = \frac{1}{2} c_{\text{even-odd}} = \frac{1}{4} c_{\text{odd-odd}} ,$$

where, unfortunately, two parameters of a and c have not been well established in magnitude due to the rather scanty experimental data. A number of values of a obtained by several authors[20-26] are at variance with each other, since the determination of a involves many difficulties. As the cross sections for different emission processes are sensitively dependent upon the magnitude of a, in addition to the above situation, we have investigated the yield of nucleons for two cases of a values, *i.e.*, those adopted by Blatt and Weisskopf[17] and by Gugelot,[21] each of which is derived from two different experimental evidences. The interpolation of Blatt and Weisskopf's a values gives us, for the nucleus concerned here,

$$a = 1.7 \text{ Mev}^{-1}, \tag{i}$$

whereas Gugelot obtained

$$a = 4.75 \text{ Mev}^{-1} \tag{ii}$$

by observing the neutron spectrum from iron excited by 16 Mev protons.

Since we have to do with the detailed distribution of excitation energies in each intermediate residual nucleus, it is convenient to introduce the branching probability $P_{ij}(E)$, as in II, which means the probability of emitting particle j from the intermediate residual nucleus left after the evaporation of particle i. If a compound nucleus can evaporate two particles in succession, the probability for emission of i and then j is

$$J_{ij} / \sum_{k,m} J_{km} , \tag{5·2}$$

where J_{ij} is defined in II. Thus, the cross section $\sigma_c(l\,;\,i,\,j)$ of the $(l\,;\,i,\,j)$ reaction is written as

$$\sigma_c(l\,;\,i,\,j) = \sigma_c^{(l)}(E_l)\,(J_{ij} / \sum_{k,m} J_{km}) . \tag{5·3}$$

$\sigma_c^{(l)}(E_l)$ is the cross section for the formation of a compound nucleus due to the particle l with incident energy E_l. Since $\sum_j P_{ij}$ is equal to unity, the sum of J_{ij} over j is rewritten as

$$\sum_j J_{ij}=F_i\,, \tag{5·4}$$

where F_i is, as defined in I, a quantity proportional to the parlial width for disintegration with emission of i. The formula (5·4) is useful in the practical calculations.

The energy spectrum of particle i emitted through the evaporation process *i.e.*, $\partial^2\sigma_c(l\,;\,i)/\partial\varepsilon_i\partial\Omega$, is given by the following formula,

$$\frac{\partial^2\sigma_c(l\,;\,i)}{\partial\varepsilon_i\partial\Omega}=\frac{\sigma_c^{(l)}(E_l)}{4\pi}\,\frac{2M_i}{\hbar}\,\frac{\varepsilon_i\sigma_c^{(i)}(\varepsilon_i)w_K^{(i)}(E_{ex}-S_i-\varepsilon_i)}{\sum_k F_k(E_{ex}-S_k)}\,, \tag{5·5}$$

where M_i is the mass of i, and $w_K^{(i)}$ the level density of the residual nucleus left after the evaporation of i.

When the first particle i is emitted with a small kinetic energy, the intermediate residual nucleus is often so highly excited that it can evaporate further a second particle to be left in the ground state or in the lower states. To obtain the experimentally observed energy spectrum, we must take into account all particles emitted from such excited nuclei. The energy spectrum of particle j emitted from the intermediate residual nucleus left after the evaporation of i will be given by

$$\frac{\partial^2\sigma_c(l\,;\,i,j)}{\partial\varepsilon_j\partial\Omega}=\frac{\sigma_i^{(l)}(E_l)}{4\pi}\,\frac{1}{\sum_k F_k}\int_0^{E_{ex}-S_i-S_{ij}-\varepsilon_j}\frac{2M_i}{\hbar^2}\cdot d\varepsilon_i\cdot\varepsilon_i\sigma_c^{(i)}(\varepsilon_i)$$

$$\times w_K^{(i)}(E_{ex}-S_i-\varepsilon_i)\,\frac{2M_j}{\hbar^2}\,\frac{\varepsilon_j\sigma_c^{(j)}(\varepsilon_j)w_K^{(i,j)}(E_{ex}-S_i-S_{ij}-\varepsilon_i)}{\sum_m F_m(E_{ex}-S_{im}-S_i-\varepsilon_i)}\,,$$

in which E_{ex} is the excitation energy of the compound nucleus, equal to E_l+S_l.

In a similar way as above, we can obtain the energy spectrum of particles evaporated from the excited residual nucleus left after a particle i is directly knocked out, as follows:

$$\frac{\partial^2\sigma_{dc}(l\,;\,i,j)}{\partial\varepsilon_j\partial\Omega}=\frac{1}{4\pi}\sum_{i=p,n}\frac{2M_j}{\hbar^2}\int_0^{E_{ex}-S_i-S_{ij}-\varepsilon_j}\frac{\partial\sigma_{di}(l\,;\,i)}{\partial\varepsilon_i}$$

$$\times\frac{\varepsilon_j\sigma_c^{(j)}(\varepsilon_j)w_K^{(i,j)}(E_{ex}-S_i-S_{ij}-\varepsilon_j)}{\sum_m F_m(E_{ex}-S_i-S_{im}-\varepsilon_j)}\,d\varepsilon_i\,. \tag{5·7}$$

Since our calculation will be concerned with the case of ^{56}Fe nuclei (the most abundant isotope of iron) bombarded by 18 Mev protons the compound nucleus will become ^{57}Co with its excitation energy equal to 18 Mev$+S_p$. In order to carry out the numerical calculations we have to know the separation energies and the cross section for the formation of the compound nucleus. The emission probability of α, d and t etc. may be taken to be negligible in magnitude, so that the emission of p, n and γ should be taken into consideration. For these cases we can employ the same cross sections as those shown in II, which have been calculated by the Feshbach-Weisskopf's formula[28] for neutrons, while, for protons, have been interporated on the table given by Blatt-Weisskopf.[27] The required separation energies are estimated by the aid of experimental resources. In fact, the threshold

Calculated cross sections are shown in Table 1

Table 1. Cross Sections for Competing Processes (Cross Section in mb)

Reaction	(i) $a=1.7$	(ii) $a=4.75$
p; n, γ	630	510
p; n, n	$<10^{-6}$	$<10^{-6}$
p; n, p	3.8	4.2
p; p, γ	140	240
p; p, n	38	60
p; p, p	1.1×10^{-3}	7.8×10^{-4}
p; n_d, γ	17	17
; n_d, n	$<10^{-6}$	$<10^{-6}$
; n_d, p	0.28	0.051
p; p_d, γ	12	12
p; p_d, n	0.15	0.057
p; p_d, p	2.1×10^{-4}	2.5×10^{-6}

of ^{56}Fe $(p\,;n)$ reactions, β-decay data, and the threshold of ^{56}Fe $(\gamma\,;n)$ reaction give us the following values for separation energies concerned :

$S_n=11.5$ Mev, $S_{np}=6.0$ Mev, $S_{nn}=?$,

$S_p=6.0$ Mev, $S_{pp}=10.8$ Mev, $S_{pn}=11.2$ Mev.

Since the value of S_{nn} can not be obtained from the experimental data, we are obliged to use the semi-empirical mass formula, which gives us 12 Mev for S_{nn}.

In the above table the suffix d stands for the particle directly knocked out. The $(p\,;2n)$ reaction is found to occur with negligible probability, because the separation energy of the first proton is much smaller than that of the first neutron. The difference between

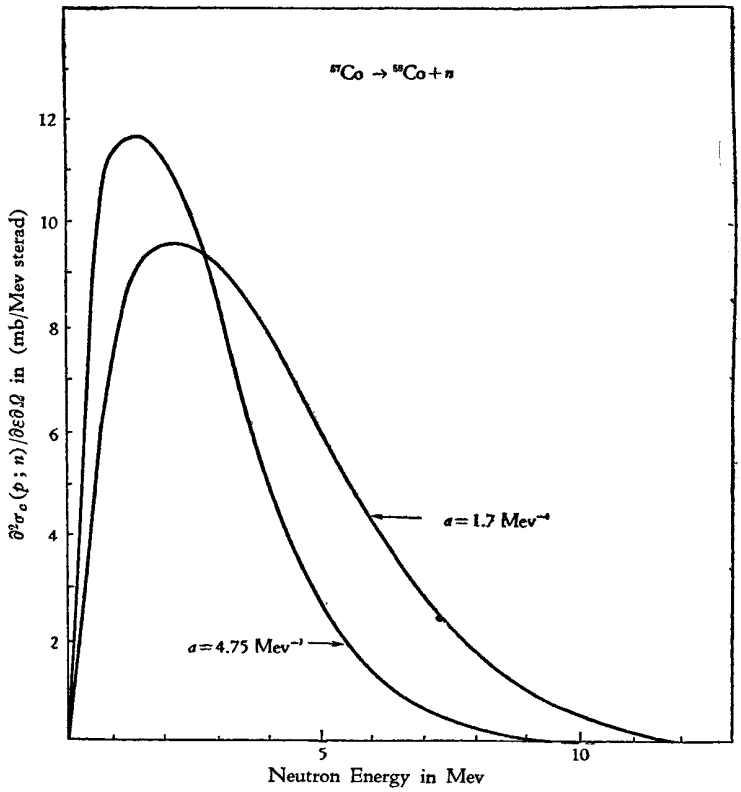

Fig. 11. Energy spectra of neutrons evaporated from the compound nucleus ^{57}Co. Curves correspond to two different a's.

these separation energies is closely related to the magnitude of the proton emission probability. If both are of the same magnitude, as is the case in most nuclei, the emission of a neutron is much more probable than that of a proton. Then the cross section for $(p\,;\,p)$ reactions fails to swell its magnitude to the one observed in most cases. Energy spectra for neutrons and protons in the respective processes are given in Fig. 11–18.

The energy spectra of particles summed over all evaporation processes are given in Fig. 19. These include the contributions from excited nuclei left after the direct interac-

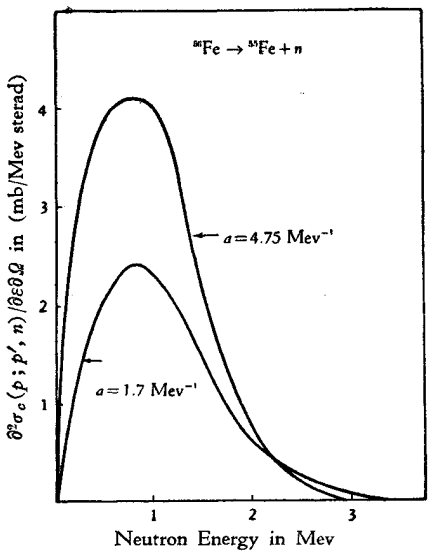

Fig. 12. Energy spectra of neutrons evaporated from intermediate residual nuclei ^{56}Fe left after the first proton evaporation. Curves correspond to two different a's.

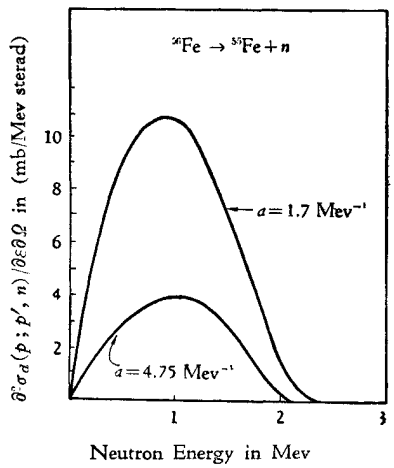

Fig. 13. Energy spectra of neutrons evaporated from excited nuclei ^{56}Fe left after the emission of protons directly knocked out. Curves correspond to two different a's.

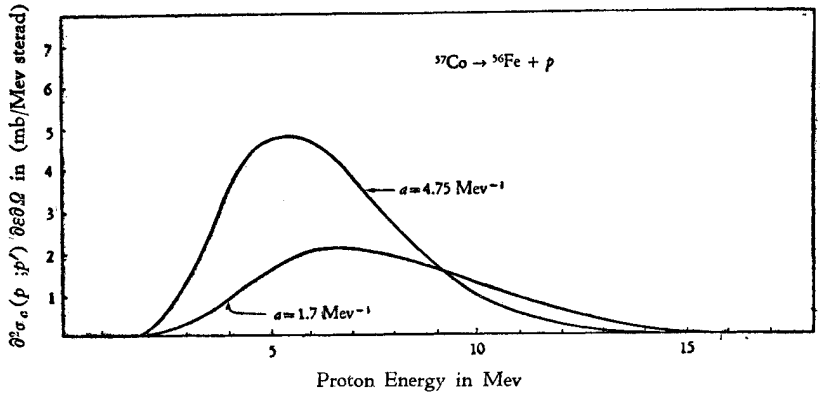

Fig. 14. Energy spectra of protons evaporated from the compound nucleus ^{57}Co. Curves correspond to two different a's.

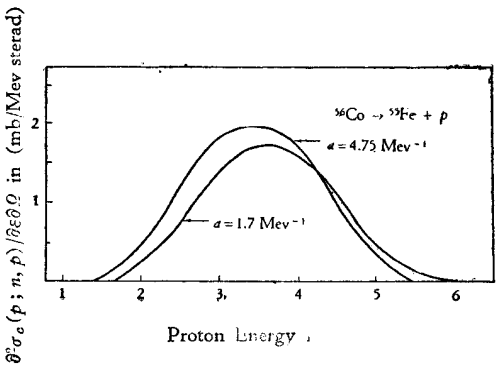

Fig. 15. Energy spectra of protons evaporated from intermediate residual nuclei ^{56}Co left after the first neutron evaporation. Curves correspond to two different a's

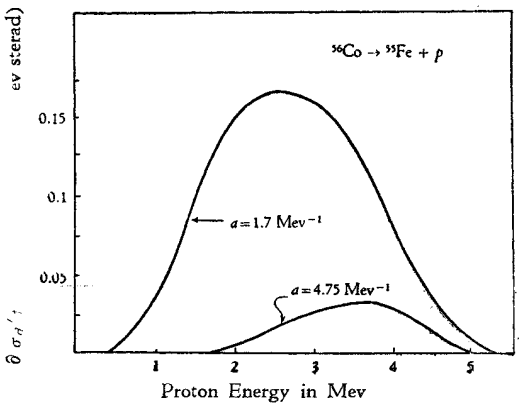

Fig. 16. Energy spectra of protons evaporated from excited nuclei ^{56}Co left after the emission of neutrons directly knocked out. Curves correspond to two different a's.

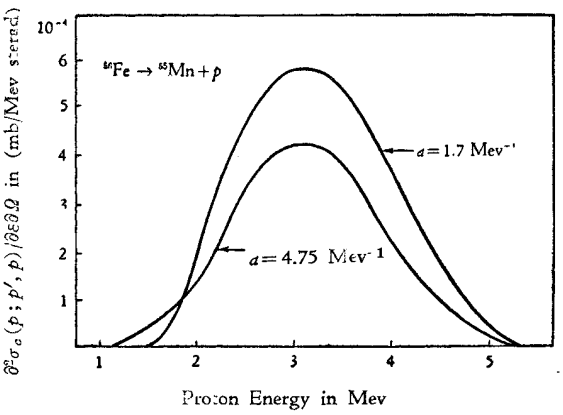

Fig. 17. Energy spectra of protons evaporated from intermediate residual nuclei ^{56}Fe left after the first proton evaporation. Curves correspond to two different a's.

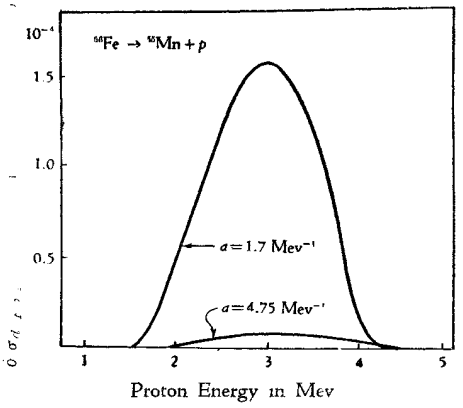

Fig. 18. Energy spectra of protons evaporated from excited nuclei ^{56}Fe left after the emission of protons directly knocked out. Curves correspond to two different a's.

tions, but do not contain those of particles directly knocked out.

The shapes of spectra obtained above are shifted from the Maxwellian type in the low energy portion, because the second nucleons in $(p\,;\,n,\,p)$ and $(p\,;\,p,\,n)$ reactions give significant contributions to the total yields. This improves considerably the agreement with the experiment at low energies, as can be seen in Fig. 19. The choice of the parameter a (ii) gives a better agreement with the experimental spectrum than that of (i).

To obtain the energy spectra corresponding to the observed one, the spectra due to the direct interaction should be added to those obtained above. As this contribution is too small, the existing discrepancy between the theoretical and the experimental results in the

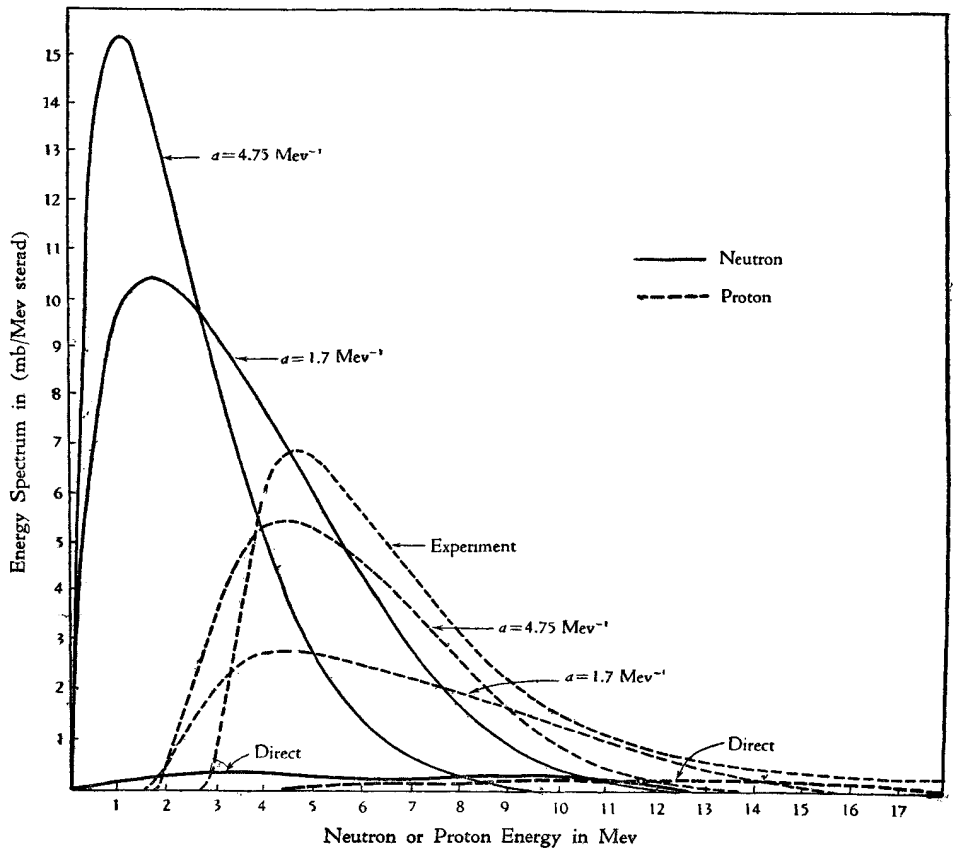

Fig. 19. Energy spectra of nucleons due to the evaporation process. Solid curve and dashed curve indicate the spectra of neutrons and protons respectively. Curves correspond to two different a's. These curves correspond to the experimental ones if being added to the contribution due to the direct process. For the comparison here are shown spectra of particles emitted at the direction of $\theta=60°$.

high energy portion can hardly be improved.

Now, the behaviour of the nuclear temperature, which depends upon the detailed property of the spectrum, shall be discussed in detail. The apparent nuclear temperature can be derived usually by neglecting the knock-out process and taking the whole energy spectrum as that due to the evaporation from the compound nucleus. The question is to examine whether the strange tendency of the nuclear temperature pointed out by Cohen[15] comes from the disregard of the direct process or not. For this purpose we have calculated the apparent nuclear temperature on the basis of the spectrum obtained in Fig. 19 and Fig. 8. Our calculation is based upon the spectrum at $\theta=60°$, while the analysis by Cohen has been performed in the backward direction ($\theta=150°$). In the backward direction the yield due to the direct process is not so large that it may not alter the energy dependence of the nuclear temperature. The apparent temperature at $\theta=60°$ is shown in Fig. 20.

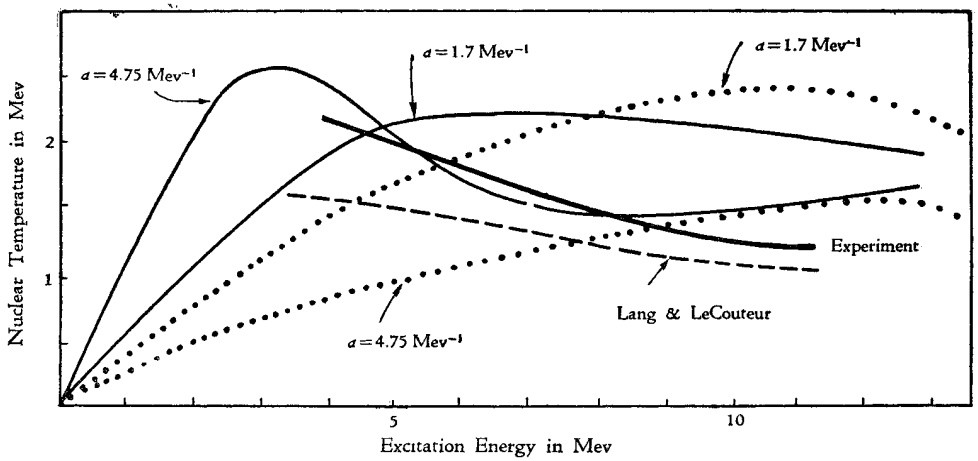

Fig. 20. Nuclear temperature (at $\Theta=60°$) derived from the spectra obtained in Fig. 19 taking into account the direct process. Curves correspond to two different a's. Dashed curve indicates the temperature corrected from the experimental spectrum by the formula given by Lang and Le Couteur.[14] Dotted curves are those derived from the spectra due to the evaporation only.

The calculated temperature approaches zero near the zero excitation energy, as it should be expected. Since the absolute value of the nuclear temperature in the Fermi gas model directly depends upon the magnitude of parameter a, the known behaviour of the temperature suggests us that a thorough analysis is required to determine the value of a from the experimental energy spectrum. Indeed, Tomasini[6] has attemped to explain the energy spectrum of neutrons by taking account of two steps of evaporation, in which two different temperatures are ascribed to respective steps and the second step is interpreted to be due possibly to the nuclear excitation left after the first neutron emission. Although this is not entirely the case in our example because of the large separation energy for neutrons, the protons evaporated from the intermediate residual nucleus after the direct neutron emission change the aspect of the proton spectrum observed in the low energy portion. From these facts it seems possible that the secondary nucleons emitted from excited nuclei left after the first nucleon evaporation or the direct nucleon emission may give an influence on the shape of the energy spectrum observed in the experiment. This effect can only take place in the low energy part of the spectrum, because the kinetic energies of secondary particles are smaller than those of the nucleons emitted from the compound nucleus. Then the nuclear temperature determined from such a range of the experimental spectrum may be lower than the actual one. Such diminishing of the temperature affected by the secondary nucleons occurs at an energy range corresponding to high excitation energies of the residual nucleus, as seen from the calculated temperature in Fig. 20.

On the other hand, Beard[29] has assumed an energy dependence of a and derived the apparent temperature that has a minimum at an excitation energy around 12 Mev. A similar behaviour of the apparent temperature can be obrained here without making such a special assumption, if a is chosen as (ii). Moreover, the choice (ii) of a gives rise to

a peak at 3 Mev due chiefly to the direct knock-out protons. This contribution alters the energy dependence of the apparent temperature, so as to decrease with increasing excitation energy. This might be thought to clarify the strange energy dependence pointed out by Cohen.[15] However, this success holds only for such protons that are scattered at 60°, but not at 150°. Nevertheless, one may suspect a possibility that some other processes could make a contribution to the backward scattering.

§ 6. Interpretation of the inelastic scattering of 31 Mev protons by Sn

The method of treatment in § 4 is so tedious that it can not always be applied to the analysis of other experimental data without much labour. In this section, therefore, we shall treat the inelastic scattering of high energy nucleons by the use of a rather simple model. We may disregard the effect of the diffraction on the nuclear surface if the energies of both incident and scattered particles are high enough.

In the above case of high energy scattering, the main feature of the process is shown schematically in Fig. 23, in which z–axis is along the direction of the incident beam and r–axis perpendicular to it. L_1 and L_2 are the lengths of paths within the nucleus before and after the collision respectively. The observed differential cross section at a direction of $\Omega(\theta, \varphi)$ is given by

$$\frac{\partial^2\sigma}{\partial\varepsilon\partial\Omega}=2\pi\int r\frac{\partial^2\sigma_{PP'}}{\partial\varepsilon\partial\Omega}\cdot\frac{L_i}{\lambda_i}\exp\left(-\frac{L_i}{\lambda_i}-\frac{L_f}{\lambda_f}\right)T_iT_f\rho(\boldsymbol{r})\,dxdrd\varphi\,, \qquad (6\cdot1)$$

where $\sigma_{PP'}$ is the cross section for the proton-nucleon scattering in nuclear matter, and λ_i and λ_f are the mean free paths for the incident and the final nucleons respectivley, T_i and T_f being the corresponding transmission coefficients. If the nucleon density $\rho(\boldsymbol{r})$ is assumed to be constant in the nucleus, (6·1) is reduced to

$$\frac{\partial^2\sigma}{\partial\varepsilon\partial\Omega}=\frac{3}{2R^3}\left(\frac{\partial^2\sigma_{PP'}}{\partial\varepsilon\partial\Omega}A\right)\int T_iT_f\frac{rL_i}{\lambda_i}\exp\left(-\frac{L_i}{\lambda_i}-\frac{L_f}{\lambda_f}\right)drdzd\varphi\,, \qquad (6\cdot2)$$

where R is the nuclear radius and A the mass number.

Further we assume T's are not dependent upon the angle of incidence on the nuclear surface but only upon the energy of particles concerned and, in the actual calculation, we take the average values for T's with the use of those given by Blatt-Weisskopf.[27]

Most of the scattered particles observed are considered to take the shortest path to emerge from the nucleus after the collision. Hence the integration with respect to φ will be performed by approximating the exponential by a Gaussian form. Since the integrals over r and z can not be done analytically, we are obliged to employ the Simpson's formula for the integration. With these approximations we have

$$\frac{\partial^2\sigma}{\partial\varepsilon\partial\Omega}=\frac{1}{2}\sqrt{\frac{\pi}{3}}\sqrt{\frac{\lambda_f}{R}}(\sin\theta)^{-1/2}\left(A\frac{\partial^2\sigma_{PP'}}{\partial\varepsilon\partial\Omega}\right)T(E_i)\,T(E_f)$$
$$\times\frac{R}{\lambda_i}\cdot\left[\frac{\sqrt{13}}{2}\frac{e^{-\frac{\sqrt{13}R}{2\lambda_i}}}{\Theta_1}-\frac{1}{2}\frac{e^{-\frac{R}{2\lambda_i}}}{\Theta_2}+\frac{4e^{-\frac{R}{\lambda_i}-\frac{R}{2\lambda_f}}\Theta_4}{\Theta_3}\right]. \qquad (6\cdot3)$$

where Θ's are complicated functions dependent only on angle θ. The values of Θ's are given in Fig. 21. $(A\partial^2\sigma_{pp'}/\partial\varepsilon\partial\Omega)$ for Sn can be calculated in a similar way to that for Fe, and the mean free path is given in Fig. 1.

The calculated cross sections are shown in Fig. 22. In spite of our rough approximation, the agreement with the experiment is fair, except for the failure to explain the proton yield in the backward direction. These particles emitted into

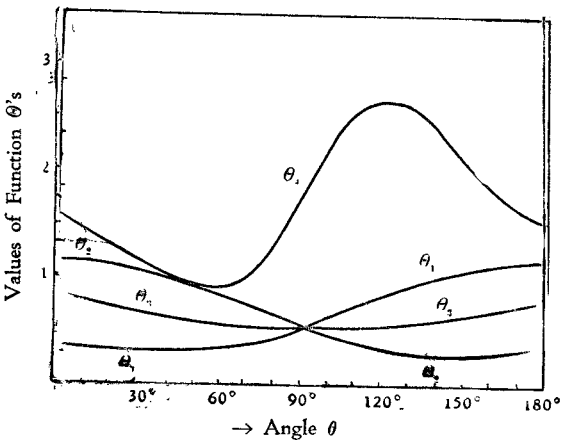

Fig. 21. Numerical values of function Θ's *vs.* angle θ.

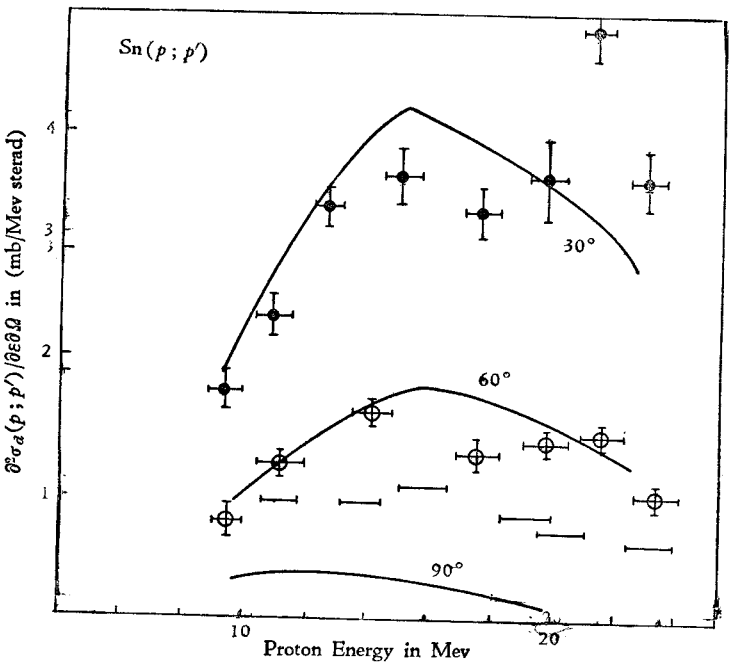

Fig. 22. Energy spectra of protons inelastically scattered by Sn. The energy of incident protons is 31 Mev. Figures attached to respective curves indicate scattered angles. Plotted experimental values are:

⊕ : $\theta=30°$

⊕ : $\theta=60°$

⊢ : $\theta=90°$

the backward direction may be due to the evaporation from the compound nucleus. This consideration is, however, rather doubtful since the proton emission is less probable than the neutron emission especially in heavy nuclei.[30,31]

The authors wish to express their hearty thanks to Prof. T. Muto for his valuable comments on this work and for the careful reading of the manuscript before publication.

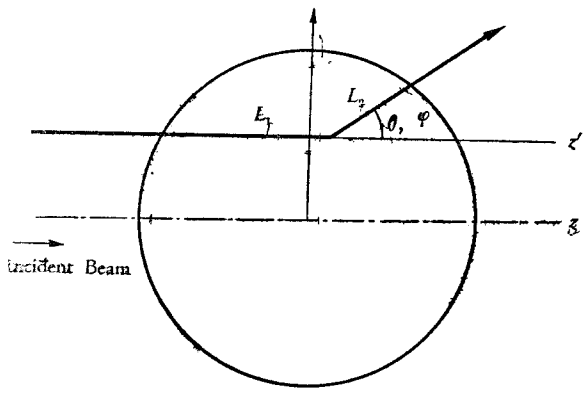

Fig. 23. Schematic representation of the inelastic scattering of high energy nucleons.

Appendix

Since our calculations developped in the text are essentially semi-classical, we adopt a semi-classical method of approximation also for the calculation of the transmission coefficients.

Let us consider first the case of neutron incidence. The component of momentum of the incident neutron along the direction of the normal to the nuclear surface at the incident point is given by

$$P_{outn}=P_{out}\cos\alpha\,, \qquad (A\cdot1)$$

where α is the incident angle. By the classical analogy, we may infer that the usual transmission coefficient for the S–wave can be taken over in our case with the modification that the momenta inside and outside the nucleus are replaced by their normal components:

$$T_n(\alpha)=\frac{4P_{outn}P_{inn}}{(P_{outn}+P_{inn})^2}\,, \qquad (A\cdot2)$$

where the suffix n signifies the normal components and P_{inn} is defined by

$$P_{inn}=P_{in}\cos\beta\,, \qquad (A\cdot3)$$

β being the angle of refraction. Now, in deriving (A·2) we have replaced approximately the spherical nuclear surface in the vicinity of the incident point by its tangent plane, which is assumed to specify a boundary of two media with different indeces of refraxion due to the nuclear potential. Further, the incident neutron beam can be supposed to be described by a plane wave with wave number vector $\boldsymbol{K}_{out}=\boldsymbol{P}_{out}/\hbar$. Solving the Schrödinger equation with the boundary condition that there should be only a transmitted wave within the nuclear side, we can easily get the transmission coefficient as described in (A·2). Thus one can see that (A·2) is the semi-classical generalization of the transmission coefficient.

In the same way as above we can calculate the transmission coefficient for incident protons. We substitute, in the expression for the S–wave transmission coefficient, the normal component of the wave number vectors in place of the wave number itself. As we are dealing with a semi-classical model, the calculation of the transmission coefficient by means

of W.K.B. approximation will be regarded reasonably to give a sufficient approximation in view of the consistency of the calculations. Then, we obtain

$$T_P(\alpha)=\frac{4k_{\mathrm{out}n}(R)\,k_{\mathrm{in}n}}{[(dk_{\mathrm{out}n}(r)/dr)/2k_{\mathrm{out}n}(r)]^2_{r=R}+(k_{\mathrm{out}n}(R)+k_{\mathrm{in}n})^2} \tag{A·3}$$

$$\text{for}\quad k^2_{\mathrm{out}n\infty}\geq\frac{a}{R},$$

$$=\frac{4\kappa_{\mathrm{out}n}(R)\,k_{\mathrm{in}n}G^{-1}}{\left(k_{\mathrm{out}n}(R)-\dfrac{a}{k_{\mathrm{out}n}(R)R}\right)^2+(k_{\mathrm{out}n}(R)\,G^{-1}+k_{\mathrm{in}n})^2} \tag{A·4}$$

$$\text{for}\quad k^2_{\mathrm{out}n\infty}\leq\frac{a}{R},$$

where $a=2M\mathcal{Z}e^2/\hbar^2$, $\mathcal{Z}$ being the atomic number of the target nucleus.

$$k_{\mathrm{out}n}(R)=\sqrt{k^2_{\mathrm{out}n\infty}-(a/R)}\,, \tag{A·5}$$

$$\kappa_{\mathrm{out}n}(R)=\sqrt{(a/R)-k^2_{\mathrm{out}n\infty}}\,, \tag{A·6}$$

$$G=\exp\left[2\int_R^b\kappa_{\mathrm{out}n}(z)\,dz\right], \tag{A·7}$$

where b is the classical turning point defined by the equation

$$k^2_{\mathrm{out}n}=\frac{a}{b} \tag{A·8}$$

and R the nuclear radius.

$T_P(\alpha)$ given above can be derived by a method which is essentially similar to that employed in the case of neutron transmission. Namely, the nuclear boundary is replaced by its tangent plane E_T at the incident point of the proton and consequently the actual Coulomb potential by the one which varies like $1/z$ outside the nucleus, z being the distance from the plane passing through the centre of the nucleus and parallel to E_T. Furthermore the spherical well of nuclear potential is substituted by a constant potential which is bounded by the plane E_T and of depth equal to that of the spherical potential. Solving the Schrödinger's equation with a proper boundary condition by means of the W.K.K. approximation, we can easily derive the above transmission coefficient. In spite of our semi-classical procedure, the transmission coefficients given above have been found to contain the wave mechanical features, although the particle with the impact parameter greater than the nuclear radius will give no contribution to the transmitted wave. This is the necessary consequence of a semi-classical model.

On the other hand the magnitude of T_p in our case is larger than the exact wave mechanical transmission coefficients for a proton with the same angular momentum. It seems to be that many partial waves with small transmission coefficients contribute to the transmitted wave by about the same amount as such partial waves allowed by classical argument. Equation (A·3) may also be regarded as a semi-classical refinement of the results obtained qy Kind and Perganini.[12]

Finally, we shall briefly discuss the path of a proton beam in the Coulomb field. In our crude approximation described above the component of a proton momentum parallel to the tangent plane E_T does not change on approaching the nuclear surface. Writing the wave number vector of the proton at an infinite distance from the nucleus by $\boldsymbol{K}_{\text{out}\infty}$, we see that the following equation holds

$$k_{\text{out}\infty t}=k_{\text{out}t}(R), \tag{A·9}$$

where the suffix t signifies the component parallel to E_T. Let the angle between the vector $\boldsymbol{K}_{\text{out}\infty}$ and the normal of E_T be η_∞, and the incident angle be η. Then, from the above equation, we have

$$k_{\text{out}\infty}\sin\eta_\infty=k_{\text{out}}(R)\sin\eta\,. \tag{A·10}$$

On the other hand the matching of wave functions in both regions at the nuclear boundary requires, as in the case of the incident neutron, the Snellius' law of refraction

$$k_{\text{out}}(R)\sin\eta=k_{\text{in}}\sin\beta \tag{A·11}$$

to hold. On account of (A·10) and (A·11) follows

$$k_{\text{out}\infty}\sin\eta_\infty=k_{\text{in}}\sin\beta\,. \tag{A·12}$$

This is the relation which we have used in (4·7) in the text.

References

1) P. C. Gugelot, Phys. Rev. **93** (1954), 425. Thanks are due to Prof. Gugelot for sending us experimental information.
2) R. M. Eisberg and G. Igo, Phys. Rev. **93** (1954), 1039.
3) R. M. Eisberg, Phys. Rev. **94** (1954), 739.
4) H. McManus and W. T. Sharp, Phys. Rev. **87** (1952), 188.
5) B. L. Cohen, E. Newman, G. A. Charpie and T. H. Handley, Phys. Rev. **94** (1954), 620.
6) M. L. Goldberger, Phys. Rev. **74** (1948), 1269.
7) G. Bernardini, E. T. Booth and S. J. Lindenbaum, Phys. Rev. **85** (1952), 826.
8) Y. Yamaguchi, Prog. Theor. Phys. **5** (1950), 332.
9) T. B. Taylor, Phys. Rev. **92** (1954), 831.
10) H. Feshbach, C. E. Porter and V. F. Wiesskopf, Phys. Rev. **90** (1953), 166; Phys. Rev. **96** (1954), 448.
11) V. F. Weisskopf, Helv. Phys. Acta, **23** (1951), 187; Science, **113** (1951), 101.
12) A. Kind and G. Perganini, Nuovo Cimento, **10** (1953), 1375.
13) N. Austern, S. T. Butler and H. McManus, Phys. Rev. **92** (1953), 350.
14) J. M. B. Lang and K. J. Le Couteur, Proc. Phys. Soc. **A67** (1954), 586.
15) B. L. Cohen, Phys. Rev. **92** (1953), 1245.
16) A. Tomasini, Nuovo Cimento, **12** (1954), 134.
17) C. C. Morrison, H. Muirhead and W. G. V. Rosser, Phil. Mag. **44** (1953), 1326.
18) S. Hayakawa and K. Kikuchi, Prog. Theor. Phys. **11** (1954), 513; cited as I.
19) S. Hayakawa and K. Kikuchi, Prog. Theor. Phys. **12** (1954), 578; cited as II.
20) P. H. Stelson and C. Goodman, Phys. Rev. **82** (1951), 69.
21) B. G. Whitmore and G. E Dennis, Phys. Rev. **84** (1951), 296.
22) E. R. Graves and L. Rosen, Phys. Rev. **89** (1953), 343.
23) R. Britten, Phys. Rev. **88** (1952), 283.
24) P. C. Gugelot, Phys. Rev. **81** (1951), 51.
25) C. S. Del Rioy Sierra and V. L. Telegdi, Phys. Rev. **90** (1953), 439.
26) E. Bleuler, A. K. Stebbins and D. J. Tendam, Phys. Rev. **90** (1953), 460.
27) J. M. Blatt and V. F. Weisskopf, *Theoretical Nucler Physics,* John Wiley and Sons, Inc. (1952).
28) H. Feshbach and V. F. Weisskopf, Phys. Rev. **76** (1949), 1550.
29) D. B. Beard, Phys. Rev. **94** (1954), 738.
30) E. B. Paul and R. L. Clarke, Can. J. Phys. **31** (1953), 267.
31) O. Hirzel and H. Wäffler, Helv. Phys. Acta, **20** (1947), 373.